



Enhanced thermoelectric performance of two dimensional MS_2 ($M = Mo, W$) through phase engineering

Bin Ouyang ^{a,*}, Shunda Chen ^b, Yuhang Jing ^{c,d}, Tianran Wei ^e, Shiyun Xiong ^{f,g,**}, Davide Donadio ^b

^a National Center for Supercomputing Applications, University of Illinois at Urbana-Champaign, Urbana, IL, 61801, United States

^b Department of Chemistry, University of California Davis, One Shields Ave, Davis, California, 95616, United States

^c Department of Astronautical Science and Mechanics, Harbin Institute of Technology, Harbin, Heilongjiang, 150001, China

^d Beckman Institute for Advanced Science and Technology, University of Illinois at Urbana-Champaign, Urbana, IL, 61801, United States

^e State Key Laboratory of High Performance Ceramics and Superfine Microstructure, Shanghai Institute of Ceramics, Chinese Academy of Sciences, Shanghai, 200050, China

^f Functional Nano and Soft Materials Laboratory (FUNSOM) and Collaborative Innovation Center of Suzhou Nano Science and Technology, Soochow University, Suzhou, Jiangsu, 215123, China

^g Max Planck Institute for Polymer Research, Ackermannweg 10, 55218, Mainz, Germany



ARTICLE INFO

Article history:

Received 1 December 2017

Received in revised form

13 July 2018

Accepted 8 August 2018

Available online 11 August 2018

Keywords:

Phase engineering

Thermoelectric

Transition metal dichalcogenides

ABSTRACT

The potential application of monolayer MS_2 ($M = Mo, W$) as thermoelectric material has been widely studied since the first report of successful fabrication. However, their performances are hindered by the considerable band gap and the large lattice thermal conductivity in the pristine 2H phase. Recent discoveries of polymorphism in MS_2 s provide new opportunities for materials engineering. In this work, phonon and electron transport properties of both 2H and 1T' phases were investigated by first-principle calculations. It is found that upon the phase transition from 2H to 1T' in MS_2 , the electron transport is greatly enhanced, while the lattice thermal conductivity is reduced by several times. These features lead to a significant enhancement of power factor by one order of magnitude in MoS_2 and by three times in WS_2 . Meanwhile, the figure of merit can reach up to 0.33 for 1T'- MoS_2 and 0.68 for 1T'- WS_2 at low temperature. These findings indicate that monolayer MS_2 in the 1T' phase can be promising materials for thermoelectric devices application. Meanwhile, this work demonstrates that phase engineering techniques can bring in one important control parameter in materials design.

© 2018 The Chinese Ceramic Society. Production and hosting by Elsevier B.V. This is an open access article under the CC BY-NC-ND license (<http://creativecommons.org/licenses/by-nc-nd/4.0/>).

1. Introduction

Monolayer MS_2 ($M = Mo$ or W) stand out of the emerging two dimensional materials majorly due to their unique electronic properties, which have inspired various applications in optoelectronics [1–6], valleytronics [7–10], and piezoelectrics [11–13]. More recently, the thermoelectric (TE) properties of monolayer MS_2 (2D- MS_2) have also been studied theoretically [8,14–22] and the

results show that they may be potential thermoelectric materials [8,14–22], in spite of a relatively large thermal conductivity (TC). However, the figure-of-merit in 2D- MS_2 needs to be further improved to be competitive with the concurrent bulk thermoelectric materials, e.g. Bi_2Te_3 [23,24], $SnSe$ [25,26] and $PbTe$ [27,28]. On one hand, the electronic band gap of 2D- MS_2 is larger than 1.5 eV [6,29] which is too large for thermoelectric application. On the other hand, the lattice TC of 2D- MS_2 should be further reduced to further improve the figure-of-merit.

More recently, the probing of polymorphism [30–34] yields a new opportunity to optimize the thermoelectric performance of MS_2 . The 2H→T structural phase transition can be triggered and stabilized through either defect engineering [33,35–38], intercalation [32,39,40] or strain engineering [31,41,42]. Previous studies suggested that 1T- MS_2 is metallic but not stable as free standing, and a Mott transition accompanied by lattice distortion occurs

* Corresponding author.

** Corresponding author. Functional Nano and Soft Materials Laboratory (FUNSOM) and Collaborative Innovation Center of Suzhou Nano Science and Technology, Soochow University, Suzhou, Jiangsu, 215123, China.

E-mail addresses: bouyang@berkeley.edu (B. Ouyang), [\(S. Xiong\).](mailto:sxiong@suda.edu.cn)

Peer review under responsibility of The Chinese Ceramic Society.

resulting in a 1T' phase with a narrow band gap [43–45]. The small electronic band gap in 1T'-MS₂ could be beneficial for electron transport due to small activation energy. Besides, the 1T' phase has a lower symmetry than the 2H phase [31], thus possibly leading to significant reductions in lattice TC. All these properties indicate that 2D MS₂ with 1T' phase could have improved thermoelectric properties compared to the 2H phase, thus might be better for energy harvesting or sensing.

Nevertheless, quantitative studies about the thermal and electron transport properties of 1T'-MS₂ are still lacking. It is then necessary to perform a systematic investigation on the thermoelectric performance of 2D MS₂ in 1T' phase. In this study, we unravel the influence of the 2H→1T' phase transition on the thermoelectric performance of MS₂s by first principles calculations. We find that the lattice TC is greatly decreased while the electron transport properties are largely enhanced in 1T'-MS₂ compared with 2H-MS₂, thus promoting about one order of magnitude enhancement of figure of merit in 1T'-MS₂ compared with 2H-MS₂ at room temperature. Specifically, the maximum figure of merit can reach 0.68 for 1T'WS₂ at the temperature of 200 K. Our theoretical findings demonstrate that 1T'-MoS₂ and 1T'-WS₂ are viable candidates for thermoelectric applications. Moreover, with various phase engineering techniques available, low dimensional thermoelectric devices with flexible and controllable properties can be achieved.

2. Methodology

2.1. Density functional theory calculations

First-principles density functional theory (DFT) calculations employing the Perdew-Burke-Ernzerhof (PBE) functional and projector augmented-wave (PAW) [46–50] method were performed using the Vienna ab initio simulation package (VASP) [51]. For electronic self-consistent calculations on electronic structure, a $47 \times 47 \times 1$ k-grid is used for obtained eigenvalues. In order to guarantee accuracy of the calculations, an energy cutoff of 800 eV is used in all calculations. The vacuum space between the monolayer and its neighboring periodic image is set to 20 Å (along the direction perpendicular to the monolayer), which is sufficient to eliminate image interactions.

2.2. Lattice thermal conductivity calculations

We use density-functional perturbation theory (DFPT) [52] as implemented in Quantum Espresso package [53] to calculate harmonic second order interatomic force constants (IFCs) with $10 \times 10 \times 1$ k-point grid and $10 \times 10 \times 1$ q-point mesh (corresponding to $10 \times 10 \times 1$ supercell) for 2H phases, and $8 \times 16 \times 1$ k-point grid and $8 \times 8 \times 1$ q-point mesh (corresponding to $8 \times 8 \times 1$ supercell) for 1T' phases.

Anharmonic third order force constants for the calculation of lattice thermal conductivity are computed by finite differences ($\Delta x = 0.01$ Å), in a $5 \times 5 \times 1$ supercell containing 75 atoms for 2H phase and in a $4 \times 4 \times 1$ supercell containing 96 atoms for 1T' phase, with a cutoff interatomic distance larger than 8 th nearest neighbor. Translational invariance is enforced using the Lagrangian approach [54].

The linearized phonon Boltzmann equation (LBTE) was solved self-consistently using ShengBTE code [54–56]. It is necessary to take iterative self-consistent (SCF) calculations, since relaxation time approximation (RTA) underestimates the thermal conductivity.

The lattice TC tensor can then be written as:

$$\kappa = \frac{1}{NV_0} \sum_{\lambda} C_{\lambda} v_{\lambda} \otimes v_{\lambda} \tau_{\lambda} \quad (1)$$

where V_0 is the volume of the unit cell, C_{λ} is the mode dependent heat capacity, v_{λ} and τ_{λ} are the group velocity and the relaxation time of the phonon mode λ respectively.

The convergence thresholds for electronic self-consistent calculation and for ionic relaxation are 10^{-16} Ry and 10^{-10} Ry/au, respectively. The convergence of thermal conductivity with q-point grids was carefully checked up to $151 \times 151 \times 1$, $27 \times 55 \times 1$, $201 \times 201 \times 1$ and $51 \times 101 \times 1$ respectively for 2H-MoS₂, 1T'-MoS₂, 2H-WS₂ and 1T'-WS₂. (Detailed convergence tests in supporting information.)

2.3. Semi-classical Boltzmann transport theory

Semi-classical Boltzmann transport theory with constant relaxation time approximation has been employed to evaluate the electron transport properties. As implemented in BOLTZTRAP code [57], the electrical conductivity and Seebeck coefficient are calculated by defining the following Fermi integrals [57]:

$$L^{(\alpha)} = e^2 \sum_n \int \frac{dk}{4\pi^3} \left(-\frac{\partial f(\epsilon_{nk})}{\partial \epsilon_{nk}} \right) \tau_n(\epsilon_{nk}) v_{nk} v_{nk} (\epsilon_{nk} - \mu)^{\alpha} \quad (2)$$

Where e is the charge of electrons and μ is the electron chemical potential, τ_n refers to the averaged relaxation time of electrons averaged by wavevector k , v_{nk} , ϵ_{nk} and $f(\epsilon_{nk})$ represent the group velocity, energy eigenvalues and Fermi-Dirac function of n th band at the wavevector k . A dense k -point mesh of $47 \times 47 \times 1$ has been adopted to obtain the Kohn-Sham energies to evaluate the transport coefficients.

2.4. Electron relaxation time calculations

The relaxation time in either armchair (AC) or zigzag (ZZ) direction can be modeled according to the Shockley's deformation potential theory:

$$\tau_{XX} = \frac{2\hbar^3 C_{XX}}{3\pi k_B T |m_{eff}| D_{XX}^2} \quad (XX = AC, ZZ) \quad (3)$$

While in equation (3) C_{XX} and D_{XX} corresponding to the stretching modulus and deformation potential constant in direction XX, respectively. The stretching modulus C_{XX} can be obtained according to the linear elastic mechanics. While D_{XX} can be computed on base on the method proposed by Bardeen and Shockley [6,8,58,59], i.e., the deformation potential tensor $D_{XX} = \Delta E/(exx)$ is determined by band energy shifting ΔE and lattice strain exx . Meanwhile, k_B and \hbar correspond to the Boltzmann constant and reduced Planck constant respectively, while T represents the temperature and m^* refers to the effective mass of electrons.

3. Results and discussion

3.1. Structure, vibrational properties and lattice TC

The atomic configurations of 2H and 1T' phases are illustrated in Fig. 1a–(b), the two-dimensional 2H-MS₂ monolayers possess a hexagonal lattice so that the optimized geometries give $a_x = a_y$. After transition from 2H phase into 1T' phase, the symmetry will break down: the top layer of S atom slides into the center of original MoS₂ hexagonal lattice, while the two adjacent Mo atoms are

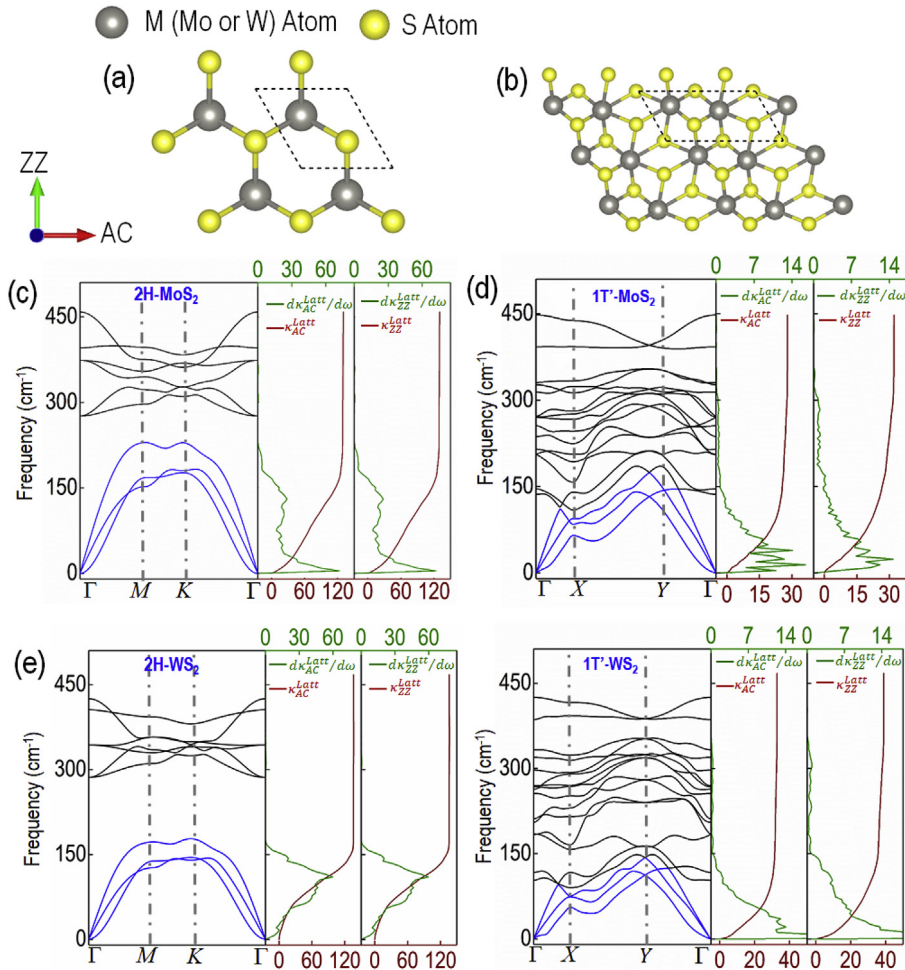


Fig. 1. Atomic configurations of MS₂ in (a) 2H phase and (b) 1T' phase, the unit cell boundaries are illustrated with dashed black lines. Phonon dispersion curves and lattice TCs of (c) 2H-MoS₂; (d) 1T'-MoS₂; (e) 2H-WS₂; (f) 1T'-WS₂. The acoustic and optical phonon branches are respectively colored with blue and black while in the accumulated lattice TC plot, the green and red lines indicate $d\kappa_{XX}^{Latt}/d\omega$ ($XX = AC$ or ZZ) and κ_{XX}^{Latt} ($XX = AC$ or ZZ), respectively. The TC is in the unit of $Wm^{-1}k^{-1}$.

dimerized to form a 2×1 supercell.

Due to the structural transition from 2H to 1T', the phonon dispersion curves of both compounds are modified dramatically. In the 2H phases, the acoustic and optical branches are separated by a gap; especially in the 2H-WS₂ structure, the phonon band gap is as large as 108 cm^{-1} . Such a large band gap limits the energy and momentum conserving phonon-phonon scattering processes, resulting in a relatively large lattice TC of 2H-WS₂. While in the 1T' phases, due to the lower symmetry and the larger number of atoms in the unit cells, the phonon band gap between optical and acoustic modes disappears completely, thus providing many more phonon scattering channels.

The vanishing of phonon band gaps enhances the density of scattering channels among acoustic and optical phonons, leading to a major reduction of phonon lifetimes. Such reduced phonon lifetimes lead to huge reduction of both κ_{AC}^{Latt} and κ_{ZZ}^{Latt} at 300 K (Table 1). The κ_{XX}^{Latt} values obtained in 1T' phases (27.9 W/mK for κ_{AC}^{Latt} and 32.2 W/mK for κ_{ZZ}^{Latt} in MoS₂ and 32.8 W/mK for κ_{AC}^{Latt} and 38.9 W/mK for κ_{ZZ}^{Latt} in WS₂) are around four times smaller than the corresponding 2H phase. The κ_{XX}^{Latt} cumulative functions with frequency (Fig. 1c–f) demonstrate that the acoustic phonons are the major contributors to the total κ_{XX}^{Latt} in 2H phases: the optical

Table 1

Calculated lattice TC in the AC direction (κ_{AC}^{Latt}) and the ZZ direction (κ_{ZZ}^{Latt}) for 2H-MS₂s, 1T'-MS₂s and optical contribution to the lattice TC in the AC direction (κ_{AC}^{Optic}) and the ZZ direction (κ_{ZZ}^{Optic}) at 300 K. The TC is in the unit of $Wm^{-1}k^{-1}$. The experimental reports are included in the brackets below.

Properties	κ_{AC}^{Latt}	κ_{ZZ}^{Latt}	$\kappa_{AC}^{Latt(Opt)}$	$\kappa_{ZZ}^{Latt(Opt)}$
2H-MoS ₂	130.3 (82 [60])	130.3 (82 [60])	1.01	1.01
1T'-MoS ₂	27.9	32.2	8.24	8.24
2H-WS ₂	136.0 (120 [60])	136.0 (120 [60])	0.18	0.18
1T'-WS ₂	32.8	38.9	9.15	9.15

phonons contribute less than 1% to the overall κ_{XX}^{Latt} . With the reduction of total κ_{XX}^{Latt} in 1T' phase, the optical contribution increases to ~20% to the overall κ_{XX}^{Latt} . It is worth mentioning that our calculated TCs for both materials are in good agreement with experimental results [15,16,18,21,60–64]. It is also worth mention that the force field based molecular dynamic simulations, will either fail to predict the metastable 1T' phase [14,65] or underestimate the thermal conductivity (Tab. S1).

Another significant difference between the 2H and 1T' phases

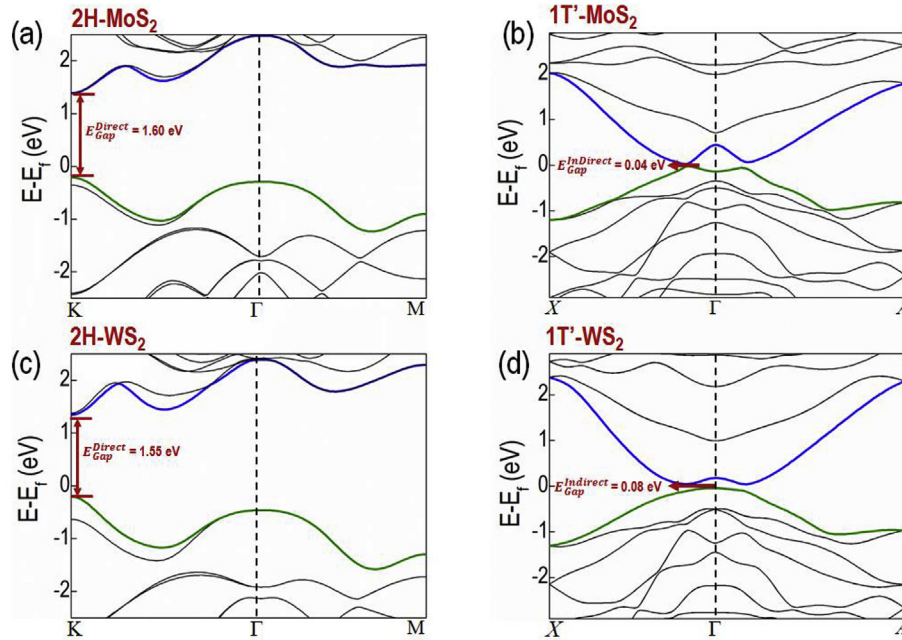


Fig. 2. Electronic band structure for (a) 2H–MoS₂; (b) 1T'–MoS₂; (c) 2H–WS₂; (d) 1T'–WS₂. The minimum conduction band and maximum covalent band are colored using olive and blue thick line separately.

is that 2H phase shows no anisotropy in TC along zigzag and armchair directions, due to the hexagonal symmetry. However, when the structure changes to 1T' phase, the $\kappa_{ZZ}^{\text{Latt}}$ of 1T' phase is larger than that of $\kappa_{AC}^{\text{Latt}}$, which makes it possible to further engineer the thermoelectric performance of 1T'-MS₂s with lattice orientations.

3.2. Electronic structure and transport properties

The electronic band structure is calculated by considering the spin-orbit coupling and the band structures of MS₂ in both 2H and 1T' phases are shown in Fig. 2. Consistent with previous calculations [6], the 2H phases exhibit large band gaps around 1.6 eV, which lead to small electrical conductivity without doping and thus make it less efficient for TE energy conversion. However, the large electronic band gaps are reduced to be smaller than 0.1 eV associating with the structural transition from 2H to 1T' phase, which are consistent with previous theoretical predictions [45] as well as experimental observations [66]. The narrowed band gaps in 1T' phase lead to dramatic enhancement of electrical conductivity, which is beneficial for TE applications. Meanwhile, the original direct band gap will transform into indirect ones.

To get more details on the electronic transport properties, the effective mass m_{eff} , τ_{XX} ($XX = AC, ZZ$) together with the deformation potentials D_{XX} , are calculated based on the

electronic band structure. As indicated in Table 2, with the transition from 2H to 1T' phase, both the effective mass and deformation potential are reduced, demonstrating that the charge carriers can travel faster and have weaker interactions with phonons in 1T' phase. As a result, the relaxation time is enhanced dramatically in both zigzag and armchair directions of both 1T'–MoS₂ and 1T'–WS₂. For the 2H phase, our calculated results are comparable to the literature results, indicating the validity of our calculations on 2H phases. While for the 1T' phase, there is no report on the effective mass, deformation potential and electron relaxation time. We realize that the relaxation times of 1T' phases are enhanced by more than one order of magnitude compared to that of the 2H phases except the zigzag direction of 1T'–WS₂. Experimental measurements demonstrated that 1T' phases are very good electrical conductor [45,67,68], however, computing the charge relaxation time for such phases using the deformation potential approach is prone to large uncertainty, due to the very narrow gap and the shape of the conduction valley. To safely estimate the electrical conductivity, we will then adopt the relaxation time of 2H phases also for the 1T' phases, which provides a conservative estimate of their electrical conductivity.

To obtain the thermoelectric properties, we calculated the electrical conductivity σ_{XX} based on the commonly used semi-classical Boltzmann transport theory, and the results are shown in Fig. 3. Due to the 2D nature of the monolayer materials we are

Table 2
Calculated effective mass m_{eff} , deformation potential constant D_{XX} , effective modulus C_{XX} , and relaxation time τ_{XX} at 300 K for different MS₂s. The reported values from literature are included in the brackets below.

Properties	$m_{\text{eff}}(m_e)$	$D_{AC}(\text{eV})$	$D_{ZZ}(\text{eV})$	$C_{AC}(\text{N/m})$	$C_{ZZ}(\text{N/m})$	$\tau_{AC}(\text{fs})$	$\tau_{ZZ}(\text{fs})$
2H–MoS ₂	0.44 (0.45 [70])	8.61	8.61	166	166	40.9 (51.7 [14])	40.9 (51.7 [14])
1T'–MoS ₂	0.11	3.71	4.89	163	149	866	455
2H–WS ₂	0.36 (0.37 [71])	9.01	9.01	180	180	50.2	50.2
1T'–WS ₂	0.27	3.24	4.67	201	122	572	167

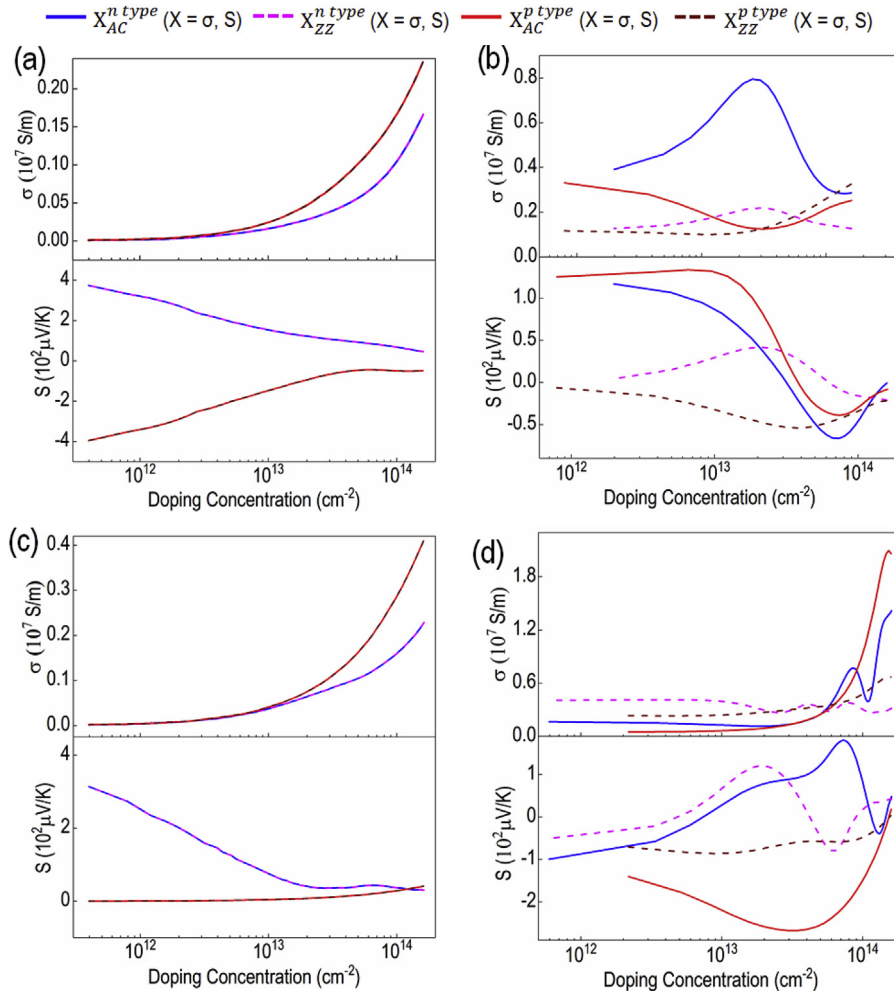


Fig. 3. Electrical conductivity σ_{XX} and Seebeck Coefficient S_{XX} as the function of the doping concentration for (a) 2H–MoS₂; (b) 1T'–MoS₂; (c) 2H–WS₂; (d) 1T'–WS₂.

discussing, the doping concentration is set as the dopant number per unit area, which takes the unit of cm^{-2} . The upper limit of doping concentration is set well below the experimental achievability ($4 \times 10^{14} \text{ cm}^{-2}$) in 2D materials [69].

The constant relaxation times obtained from DFT calculations are used to evaluate the electrical conductivity. As mentioned above, the relaxation time of the corresponding 2H phases are adopted for the electrical conductivity calculation of 1T' phase as a very conservative estimation. As illustrated in Fig. 3, σ_{XX} increases with the increase of doping concentration in 2H–MS₂s, and the obtained values agree with previous reports [14]. The 2H → 1T' phase transition significantly changes the electrical conductivity, which varies non-monotonically with doping concentration. However, in general, the electrical conductivity in 1T' phase is greatly enhanced compared to that of the 2H phase. Such improvement can be attributed to the shrinkage of band gap and reduction of effective mass since the same relaxation time is adopted.

Meanwhile, the Seebeck coefficient of the two compounds is slightly reduced at low doping concentrations due to the 2H → 1T' phase transition. Such reduction of S stems from the narrowed band gap of 1T'–MS₂s, which makes them behave similar to metals. However, with the increase of doping concentration, the S_{XX} of 2H–MS₂s will be comparable with those of 1T'–MS₂s. This indicates that the power factor (σS^2) should be considerably enhanced at

optimized doping concentrations.

3.3. Power factor and figure of merit

With all the values obtained above, the thermoelectric performance of 1T'–MS₂s and 2H–MS₂ can be evaluated. The power factor (PF) taking the form $PF_{XX} = \sigma_{XX} S_{XX}^2$ and the figure of merit $ZT_{XX} = \sigma_{XX} S_{XX}^2 T / (\kappa_{XX}^e + \kappa_{XX}^{latt})$ are calculated and the obtained results are demonstrated in Fig. 4. Being consistent with previous theoretical calculations [14,19,70], PF_{XX} and ZT_{XX} for 2H–MoS₂ are no more than $0.005 \text{ W m}^{-1} \text{ K}^{-2}$ and 0.012 respectively at 300 K (Fig. 4a), which is quite low to serve as ideal thermoelectric materials. Similarly, 2H–WS₂ (Fig. 4b) possesses PF_{XX} no more than $0.12 \text{ W m}^{-1} \text{ K}^{-2}$ and ZT_{XX} smaller than 0.05 . However, with the phase transition from 2H → 1T', both PF_{XX} and ZT_{XX} are greatly improved for both p-type and n-type doping. Particularly, PF_{XX} for n-type doped 1T'–MoS₂ reaches the maximum of around $0.053 \text{ W m}^{-1} \text{ K}^{-2}$ while the peak ZT can be as large as 0.27 . Those values turn out to be 10 times and 23 times higher than those of 2H phase. For p-type doped 1T'–MoS₂, the peak ZT can also reach around 0.1 in both AC and ZZ directions. The large ZT value of n-type doped 1T'–MoS₂ indicates that it is a good n-type TE material. For n-type doped 1T'–WS₂, similar with 1T'–MoS₂, the peak power factor is much higher than for p-type. Nevertheless, the peak ZT of p-type doped 1T'–WS₂ in the AC direction is

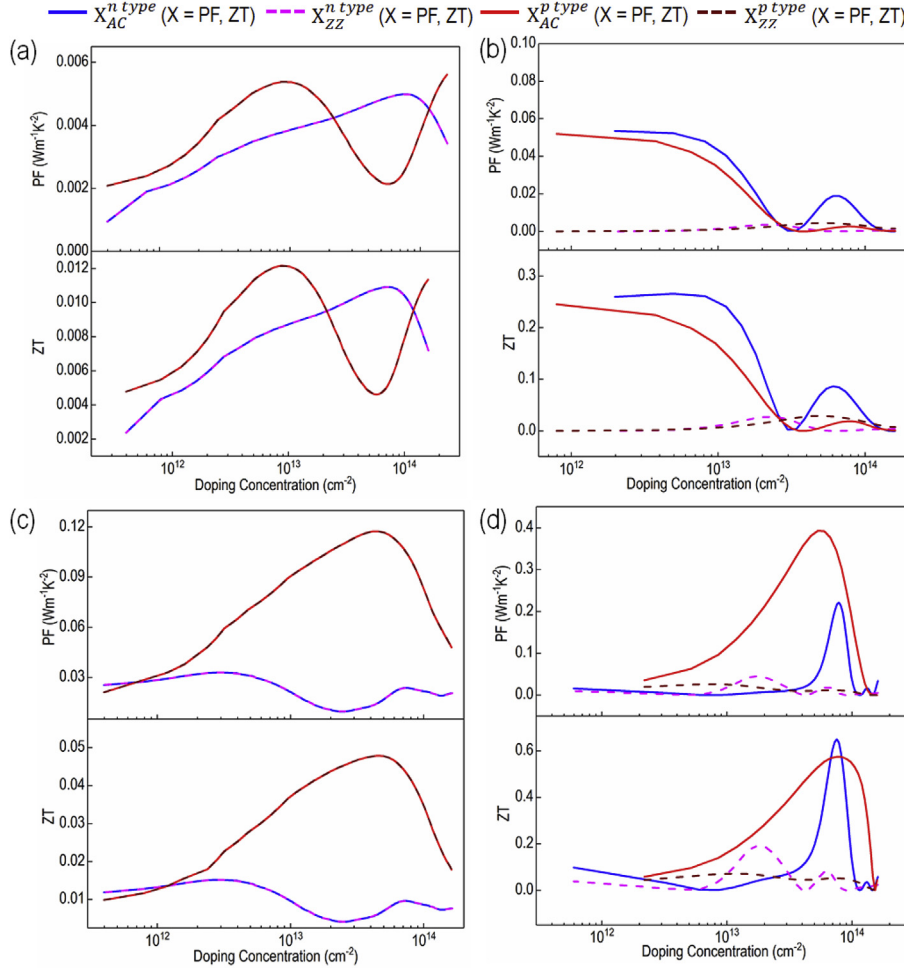


Fig. 4. Power factor PF_{XX} and figure of merit ZT_{XX} for (a) 2H–MoS₂; (b) 1T'–MoS₂; (c) 2H–WS₂; (d) 1T'–WS₂.

comparable to that of n-type doped. And the best ZT can reach up to 0.65, 13 times larger than that of 2H–WS₂ and comparable to many state-of-art TE materials [72–74]. This result also indicates that 1T'–WS₂ can be good TE material for both n-type and p-type applications, but when used for p-type TE material, one should specifically choose the AC direction to maximize the energy conversion efficiency. This large anisotropy of ZT value in AC and ZZ direction also gives the possibility for further enhance the TE figure-of-merit, e.g., fabricate nanoribbons in the AC direction. It is also worth mentioning that the significant improvements of thermoelectric efficiency not only origin from the decrease of lattice thermal conductivity, but also come from the great enhancement of electron transport. The significant enhancement of electron transport in two-dimensional transition metal chalcogenides have already been reported and demonstrated both experimentally and theoretically in the literature [45,67,68].

Since TE materials are served in a temperature range, we have also studied the temperature effect of ZT for both 2H–MS₂s and 1T'–MS₂. The ZT value in the temperature range from 200 K to 800 K is evaluated in Fig. 5(b)–(e). The doping concentration with highest ZT_{XX} under 300 K are chosen to illustrate the limit of performance. It is shown in Fig. 5(b) that the maximum ZT_{XX} stays 0.02 at 400 K for 2H–MoS₂ and further elevation of temperature will reduce ZT_{XX} . On the other hand, the ZT_{XX} of 2H–WS₂

will be monotonically elevated at the temperature region studied (Fig. 5c) with the highest value of 0.16 at 800 K. Different from 2H–MS₂, by increasing temperature, the values of ZT_{XX} will generally drop except for a bit increase after 480 K for ZT_{ZZ} of 1T'–MoS₂ (Fig. 5c). Meanwhile, the maximum ZT_{XX} can be reached is 0.33 and 0.68 for 1T'–MoS₂ and 1T'–WS₂ respectively. Those results indicate that the 1T' MS₂ are good candidates for low temperature TE performance.

Furthermore, another interesting phenomenon should be mentioned with Figs. 4 and 5 is that the improvement of performance due to 2H→1T' transition is always greater in WS₂ rather than MoS₂; meanwhile, 1T'–WS₂ usually shows higher ZT_{XX} value when compared with 1T'–MoS₂. To be more specific, with the change of temperature, the highest ZT_{XX} value can reach around 0.33 for 1T'–MoS₂ and 0.68 for 1T'–WS₂. All those observations reveal the fact that 1T'–WS₂ yields better potential serving in thermoelectric devices.

4. Summary

To conclude, the thermal properties and thermoelectric performance of MS₂s are studied utilizing first principle theoretical calculations together with relevant transport theories. It has been found out that the 2H→1T' phase transition will induce

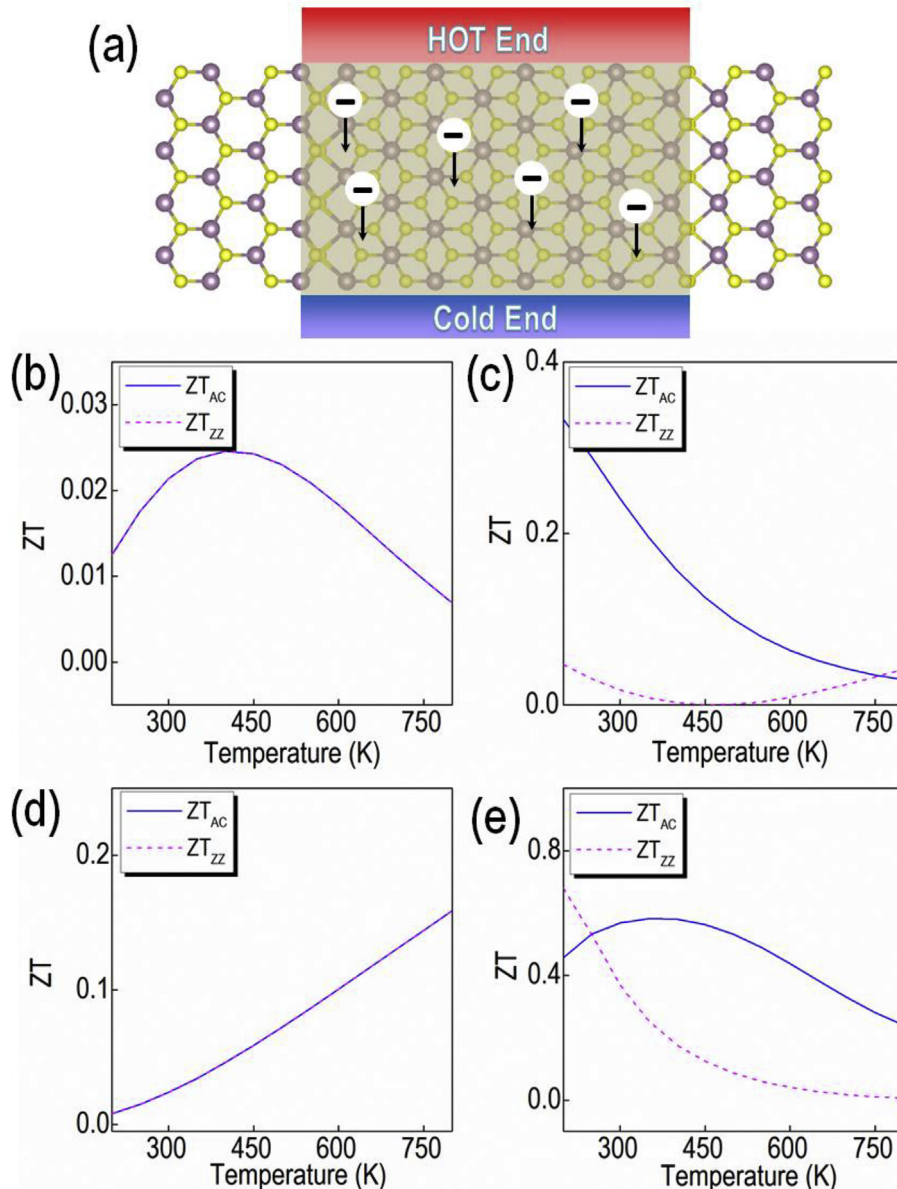


Fig. 5. (a) Illustration of improved thermal response with inducing phase transition; figure of merit versus temperature for (b) 2H–MoS₂; (c) 1T'–MoS₂; (d) 2H–WS₂; (e) 1T'–WS₂. The doping concentrations with highest ZT are selected for each material.

significantly lower lattice TC, and much higher electrical conductivity, which lead to enhanced thermoelectric performance in 1T' phase. With optimized doping concentration, the TE figure of merit in MoS₂ and WS₂ can reach to 0.33 and 0.68 respectively. With the state-of-the-art techniques to control phase transformation, our studies suggest a new application within 1T' phase of MS₂ and proposes two new candidates (1T'–MoS₂ and 1T'–WS₂) as potential thermoelectric materials. All these theoretical insights will provide valuable information for the design of new efficient low-dimensional thermoelectric devices employing 2D-MS₂.

Acknowledgements

This work is supported by the Jiangsu provincial natural science

funding Project (No. BK20160308) and the NSF of Heilongjiang Province of China under Grants No. QC2015001.

Appendix A. Supplementary data

Supplementary data related to this article can be found at <https://doi.org/10.1016/j.jmat.2018.08.001>.

References

- [1] Bernardi M, Palummo M, Grossman JC. Extraordinary sunlight absorption and one nanometer thick photovoltaics using two-dimensional monolayer materials. *Nano Lett* 2013;13(8):3664–70.
- [2] Buscema M, Barkelid M, Zwiller V, van der Zant HSJ, Steele GA, Castellanos-Gomez A. Large and tunable photothermoelectric effect in single-layer MoS₂. *Nano Lett* 2013;13(2):358–63.
- [3] Feng J, Qian X, Huang C-W, Li J. Strain-engineered artificial atom as a broad-

- spectrum solar energy funnel. *Nat Photon* 2012;6(12):866–72.
- [4] Huang S, Ling X, Liang L, Kong J, Terrones H, Meunier V, Dresselhaus MS. Probing the interlayer coupling of twisted bilayer MoS₂ using photoluminescence spectroscopy. *Nano Lett* 2014;14(10):5500–8.
 - [5] Splendiani A, Sun L, Zhang Y, Li T, Kim J, Chim C-Y, Galli G, Wang F. Emerging photoluminescence in monolayer MoS₂. *Nano Lett* 2010;10(4):1271–5.
 - [6] Ouyang B, Mi Z, Song J. Bandgap transition of 2H transition metal dichalcogenides: predictive tuning via inherent interface coupling and strain. *J Phys Chem C* 2016;120(16):8927–35.
 - [7] Mak KF, He K, Lee C, Lee GH, Hone J, Heinz TF, Shan J. Tightly bound trions in monolayer MoS₂. *Nat Mater* 2013;12(3):207–11.
 - [8] He K, Kumar N, Zhao L, Wang Z, Mak KF, Zhao H, Shan J. Tightly bound excitons in monolayer WSe₂. *Phys Rev Lett* 2014;113(2):026803.
 - [9] MacNeill D, Heikes C, Mak KF, Anderson Z, Kormányos A, Zólyomi V, Park J, Ralph DC. Breaking of valley degeneracy by magnetic field in monolayer MoSe₂. *Phys Rev Lett* 2015;114(3):037401.
 - [10] Xiao D, Liu G-B, Feng W, Xu X, Yao W. Coupled spin and valley physics in monolayers of MoS₂ and other group-VI dichalcogenides. *Phys Rev Lett* 2012;108(19):196802.
 - [11] Wu T, Zhang H. Piezoelektrizität in zweidimensionalen materialien. *Angew Chem* 2015;127(15):4508–10.
 - [12] Reed EJ. Piezoelectricity: now in two dimensions. *Nat Nanotechnol* 2015;10(2):106–7.
 - [13] Wu W, Wang L, Li Y, Zhang F, Lin L, Niu S, Chenet D, Zhang X, Hao Y, Heinz TF, Hone J, Wang ZL. Piezoelectricity of single-atomic-layer MoS₂ for energy conversion and piezotronics. *Nature* 2014;514(7523):470–4.
 - [14] Jin Z, Liao Q, Fang H, Liu Z, Liu W, Ding Z, Luo T, Yang N. A revisit to high thermoelectric performance of single-layer MoS₂. *Sci Rep* 2015;5:18342.
 - [15] Huang W, Luo X, Gan CK, Quek SY, Liang G. Theoretical study of thermoelectric properties of few-layer MoS₂ and WSe₂. *Phys Chem Chem Phys* 2014;16(22):10866–74.
 - [16] Arab A, Li Q. Anisotropic thermoelectric behavior in armchair and zigzag mono- and fewlayer MoS₂ in thermoelectric generator applications. *Sci Rep* 2015;5:13706.
 - [17] Sevik C. Assessment on lattice thermal properties of two-dimensional honeycomb structures: graphene, h-BN, h-MoS₂, and h-MoSe₂. *Phys Rev B* 2014;89(3):035422.
 - [18] Tahir M, Schwingenschlögl U. Tunable thermoelectricity in monolayers of MoS₂ and other group-VI dichalcogenides. *N J Phys* 2014;16(11):115003.
 - [19] Gandi AN, Schwingenschlögl U. WS₂ as an excellent high-temperature thermoelectric material. *Chem Mater* 2014;26(22):6628–37.
 - [20] Yan R, Simpson JR, Bertolazzi S, Brivio J, Watson M, Wu X, Kis A, Luo T, Hight Walker AR, Xing HG. Thermal conductivity of monolayer molybdenum disulfide obtained from temperature-dependent Raman spectroscopy. *ACS Nano* 2014;8(1):986–93.
 - [21] Gu X, Li B, Yang R. Layer thickness-dependent phonon properties and thermal conductivity of MoS₂. *J Appl Phys* 2016;119(8):085106.
 - [22] Peimyoo N, Shang J, Yang W, Wang Y, Cong C, Yu T. Thermal conductivity determination of suspended mono- and bilayer WS₂ by Raman spectroscopy. *Nano Res* 2015;8(4):1210–21.
 - [23] Yang L, Chen Z-G, Hong M, Han G, Zou J. Enhanced thermoelectric performance of nanostructured Bi₂Te₃ through significant phonon scattering. *ACS Appl Mater Interfaces* 2015;7(42):23694–9.
 - [24] Wright DA. Thermoelectric properties of bismuth telluride and its alloys. *Nature* 1958;181(4612):834–834.
 - [25] Zhao L-D, Lo S-H, Zhang Y, Sun H, Tan G, Uher C, Wolverton C, Dravid VP, Kanatzidis MG. Ultralow thermal conductivity and high thermoelectric figure of merit in SnSe crystals. *Nature* 2014;508(7496):373–7.
 - [26] Zhao L-D, Chang C, Tan G, Kanatzidis MG. SnSe: a remarkable new thermoelectric material. *Energy Environ Sci* 2016;9(10):3044–60.
 - [27] Heremans JP, Jovovic V, Toberer ES, Saramat A, Kurosaki K, Charoenphakdee A, Yamanaka S, Snyder GJ. Enhancement of thermoelectric efficiency in PbTe by distortion of the electronic density of states. *Science* 2008;321(5888):554–7.
 - [28] Pei Y, Wang H, Snyder GJ. Band engineering of thermoelectric materials. *Adv Mater* 2012;24(46):6125–35.
 - [29] Mak KF, Lee C, Hone J, Heinz TF. Atomically thin MoS₂: a new direct-gap semiconductor. *Phys Rev Lett* 2010;105(13):136805.
 - [30] Eda G, Fujita T, Yamaguchi H, Voiry D, Chen M, Chhowalla M. Coherent atomic and electronic heterostructures of single-layer MoS₂. *ACS Nano* 2012;6(8):7311–7.
 - [31] Ouyang B, Lan G, Guo Y, Mi Z, Song J. Phase engineering of monolayer transition-metal dichalcogenide through coupled electron doping and lattice deformation. *Appl Phys Lett* 2015;107(19):191903.
 - [32] Guo Y, Sun D, Ouyang B, Raja A, Song J, Heinz TF, Brus LE. Probing the dynamics of the metallic-to-semiconducting structural phase transformation in MoS₂ crystals. *Nano Lett* 2015;15(8):5081–8.
 - [33] Lin Y-C, Dumcenco DO, Huang Y-S, Suenaga K. Atomic mechanism of the semiconducting-to-metallic phase transition in single-layered MoS₂. *Nat Nanotechnol* 2014;9(5):391–6.
 - [34] Ouyang B, Xiong S, Yang Z, Jing Y, Wang Y. MoS₂ heterostructure with tunable phase stability: strain induced interlayer covalent bond formation. *Nanoscale* 2017;9(24):8126–32.
 - [35] Cai L, He J, Liu Q, Yao T, Chen L, Yan W, Hu F, Jiang Y, Zhao Y, Hu T, Sun Z, Wei S. Vacancy-Induced ferromagnetism of MoS₂ nanosheets. *J Am Chem Soc* 2015;137(7):2622–7.
 - [36] Zhou Y, Reed EJ. Structural phase stability control of monolayer MoTe₂ with adsorbed atoms and molecules. *J Phys Chem C* 2015;119(37):21674–80.
 - [37] Ouyang B, Ou P, Wang Y, Mi Z, Song J. Phase engineering of MoS₂ through GaN/AlN substrate coupling and electron doping. *Phys Chem Chem Phys* 2016;18(48):33351–6.
 - [38] Ouyang B, Xiong S, Jing Y. Tunable phase stability and contact resistance of monolayer transition metal dichalcogenides contacts with metal. *npj 2D Mater Appl* 2018;2(1):13.
 - [39] Enyashin AN, Yadgarov L, Houben L, Popov I, Weidenbach M, Tenne R, Bar-Sadan M, Seifert G. New route for stabilization of 1t-WS₂ and MoS₂ phases. *J Phys Chem C* 2011;115(50):24586–91.
 - [40] Kappera R, Voiry D, Yalcin SE, Branch B, Gupta G, Mohite AD, Chhowalla M. Phase-engineered low-resistance contacts for ultrathin MoS₂ transistors. *Nat Mater* 2014;13(12):1128–34.
 - [41] Duerloo K-AN, Li Y, Reed EJ. Structural phase transitions in two-dimensional Mo- and W-dichalcogenide monolayers. *Nat Commun* 2014;5.
 - [42] Ouyang B, Ou P, Song J. Controllable phase stabilities in transition metal dichalcogenides through curvature engineering: first-principles calculations and continuum prediction. *Adv Theor Simul* 2018;1(6):1800003.
 - [43] Du H, Guo H-L, Liu Y-N, Xie X, Liang K, Zhou X, Wang X, Xu A-W. Metallic 1t-LixMoS₂ cocatalyst significantly enhanced the photocatalytic H₂ evolution over Cd0.5Zn0.5S nanocrystals under visible light irradiation. *ACS Appl Mater Interfaces* 2016;8(6):4023–30.
 - [44] Lukowski MA, Daniel AS, Meng F, Forticaux A, Li L, Jin S. Enhanced hydrogen evolution catalysis from chemically exfoliated metallic MoS₂ nanosheets. *J Am Chem Soc* 2013;135(28):10274–7.
 - [45] Qian X, Liu J, Fu L, Li J. Quantum spin Hall effect in two-dimensional transition metal dichalcogenides. *Science* 2014;346(6215):1344–7.
 - [46] Hohenberg P, Kohn W. Inhomogeneous electron gas. *Phys Rev* 1964;136(3B):B864–71.
 - [47] Kohn W, Sham LJ. Self-consistent equations including exchange and correlation effects. *Phys Rev* 1965;140(4A):A1133–8.
 - [48] Blöchl PE. Projector augmented-wave method. *Phys Rev B* 1994;50(24):17953–79.
 - [49] Kresse G, Furthmüller J. Efficient iterative schemes for ab initio total-energy calculations using a plane-wave basis set. *Phys Rev B* 1996;54(16):11169–86.
 - [50] Perdew JP, Burke K, Ernzerhof M. Generalized gradient approximation made simple. *Phys Rev Lett* 1996;77(18):3865–8.
 - [51] Lu N, Guo H, Li L, Dai J, Wang L, Mei W-N, Wu X, Zeng XC. MoS₂/MX₂ heterobilayers: bandgap engineering via tensile strain or external electrical field. *Nanoscale* 2014;6(5):2879–86.
 - [52] Baroni S, de Gironcoli S, Dal Corso A, Giannozzi P. Phonons and related crystal properties from density-functional perturbation theory. *Rev Mod Phys* 2001;73(2):515–62.
 - [53] Paolo G, Stefano B, Nicola B, Matteo C, Roberto C, Carlo C, Davide C, Guido LC, Matteo C, Ismaila D, Andrea Dal C, Stefano de G, Stefano F, Guido F, Ralph G, Uwe G, Christos G, Anton K, Michele L, Layla M-S, Nicola M, Francesco M, Riccardo M, Stefano P, Alfredo P, Lorenzo P, Carlo P, Sandro S, Gabriele S, Ari PS, Alexander S, Paolo U, Renata MW. QUANTUM ESPRESSO: a modular and open-source software project for quantum simulations of materials. *J Phys Condens Matter* 2009;21(39):395502.
 - [54] Li W, Carrete J, Katcho NA, Mingo N, ShengBTE. A solver of the Boltzmann transport equation for phonons. *Comput Phys Commun* 2014;185(6):1747–58.
 - [55] Li W, Mingo N, Lindsay L, Broido DA, Stewart DA, Katcho NA. Thermal conductivity of diamond nanowires from first principles. *Phys Rev B* 2012;85(19):195436.
 - [56] Li W, Lindsay L, Broido DA, Stewart DA, Mingo N. Thermal conductivity of bulk and nanowire Mg₂SixSn_{1-x} alloys from first principles. *Phys Rev B* 2012;86(17):174307.
 - [57] Madsen GK, Singh DJ. BoltzTraP. A code for calculating band-structure dependent quantities. *Comput Phys Commun* 2006;175(1):67–71.
 - [58] Cai Y, Zhang G, Zhang Y-W. Polarity-reversed robust Carrier mobility in monolayer MoS₂ nanoribbons. *J Am Chem Soc* 2014;136(17):6269–75.
 - [59] Bardeen J, Shockley W. Deformation potentials and mobilities in non-polar crystals. *Phys Rev* 1950;80(1):72–80.
 - [60] Jiang P, Qian X, Gu X, Yang R. Probing anisotropic thermal conductivity of transition metal dichalcogenides MX₂ (M = Mo, W and X = S, Se) using time-domain thermoreflectance. *Adv Mater* 2017;29(36):1701068.
 - [61] Lindroth DO, Erhart P. Thermal transport in van der Waals solids from first-principles calculations. *Phys Rev B* 2016;94(11):115205.
 - [62] Zhu G, Liu J, Zheng Q, Zhang R, Li D, Banerjee D, Cahill DG. Tuning thermal conductivity in molybdenum disulfide by electrochemical intercalation. *Nat Commun* 2016;7:13211.
 - [63] Zhang X, Sun D, Li Y, Lee G-H, Cui X, Chenet D, You Y, Heinz TF, Hone JC. Measurement of lateral and interfacial thermal conductivity of single- and bilayer MoS₂ and MoSe₂ using refined optothermal Raman technique. *ACS Appl Mater Interfaces* 2015;7(46):25923–9.
 - [64] Gu X, Yang R. Phonon transport in single-layer transition metal dichalcogenides: a first-principles study. *Appl Phys Lett* 2014;105(13):131903.
 - [65] Jiang J-W, Park H, Rabczuk T. Molecular dynamics simulations of single-layer

- molybdenum disulphide (MoS₂): stillinger-Weber parametrization, mechanical properties, and thermal conductivity. *J Appl Phys* 2013;114(6). 064307.
- [66] Tan SJR, Abdelwahab I, Ding Z, Zhao X, Yang T, Loke GZJ, Lin H, Verzhbitskiy I, Poh SM, Xu H, Nai CT, Zhou W, Eda G, Jia B, Loh KP. Chemical stabilization of 1T' phase transition metal dichalcogenides with giant optical Kerr nonlinearity. *J Am Chem Soc* 2017;139(6):2504–11.
- [67] Kang D, Zhou Y, Yi W, Yang C, Guo J, Shi Y, Zhang S, Wang Z, Zhang C, Jiang S, Li A, Yang K, Wu Q, Zhang G, Sun L, Zhao Z. Superconductivity emerging from a suppressed large magnetoresistant state in tungsten ditelluride. *Nat Commun* 2015;6:7804.
- [68] Pan X-C, Chen X, Liu H, Feng Y, Wei Z, Zhou Y, Chi Z, Pi L, Yen F, Song F, Wan X, Yang Z, Wang B, Wang G, Zhang Y. Pressure-driven dome-shaped superconductivity and electronic structural evolution in tungsten ditelluride. *Nat Commun* 2015;6:7805.
- [69] Efetov DK, Kim P. Controlling electron-phonon interactions in graphene at ultrahigh carrier densities. *Phys Rev Lett* 2010;105(25). 256805.
- [70] Babaei H, Khodadadi JM, Sinha S. Large theoretical thermoelectric power factor of suspended single-layer MoS₂. *Appl Phys Lett* 2014;105(19). 193901.
- [71] Zhu B, Chen X, Cui X. Exciton binding energy of monolayer WS₂. *Sci Rep* 2015;5:9218.
- [72] Lee EK, Yin L, Lee Y, Lee JW, Lee SJ, Lee J, Cha SN, Whang D, Hwang GS, Hippalgaonkar K, Majumdar A, Yu C, Choi BL, Kim JM, Kim K. Large thermoelectric figure-of-merits from SiGe nanowires by simultaneously measuring electrical and thermal transport properties. *Nano Lett* 2012;12(6):2918–23.
- [73] Zhao L-D, David VP, Kanatzidis MG. The panoscopic approach to high performance thermoelectrics. *Energy Environ Sci* 2014;7(1):251–68.
- [74] Wan C, Gu X, Dang F, Itoh T, Wang Y, Sasaki H, Kondo M, Koga K, Yabuki K, Snyder GJ, Yang R, Koumoto K. Flexible n-type thermoelectric materials by organic intercalation of layered transition metal dichalcogenide TiS₂. *Nat Mater* 2015;14(6):622–7.



Dr. Bin Ouyang is a postdoctoral research associate working in National Center for Supercomputing Applications at University of Illinois at Urbana-Champaign. He received his B. Eng in Materials Science and Engineering at Central South University in Changsha, China. After which he obtained his Ph. D degree at McGill University in Montreal, Canada. His research focus is on phase transitions, thermodynamic properties as well as electron and thermal transport properties within solids.



Prof. Shiyun Xiong is currently an associate Professor of the Institute of Functional Nano and Soft Materials at Soochow University. Prof. Xiong's main research interests include but not limited to theoretical studies on nanoscale heat transfer, charge transport in optoelectronics. He received his BS and MS degrees in materials physics and chemistry from Central South University (China) in 2009 and 2011, respectively. Afterwards, he joined Ecole Centrale Paris in France and obtained his Ph.D degree in physics engineering in 2014. After his Ph.D studies, Prof. Xiong joined the Max-Planck Institute for Polymer Research as a postdoc research fellow and was sponsored by the Alexander von Humboldt foundation for his postdoc research. Since 2017, Prof. Xiong has been working at the Institute of Functional Nano and Soft Materials at Soochow University, Soochow University.